# On the Vibrations of a MEMS Gyroscope

**Wyatt O. Davis and Albert P. Pisano**

Berkeley Sensor and Actuator Center, University of California
at Berkeley (wdavis@me.berkeley.edu)

## Abstract

In this paper, the dynamics of a dual-axis MEMS gyroscope are examined. The model for the device is based on a non-linear rod theory developed by A. E. Green, P. M. Naghdi and several co-workers. A preliminary analysis of the model, which presumes certain symmetries and small deformations, is used to examine three particular modes of operation of the device. These modes are the sensor's drive mode, tilt mode, and bounce mode. Such an analysis is a necessary precursor to the more difficult task of analyzing the effects of design imperfections on the dynamics of this device.

**Keywords:** Gyroscope, rate sensor, beam vibration.

## Introduction

MEMS gyroscope designs are typically based on vibrations of a proof mass suspended on elastic tethers since bearings on the microscale are not yet feasible for this application. The design shown in Figure 1 possesses an inherent symmetry which provides two input axes [1]. Unlike single input axis gyroscopes, the motion of the tethers is three-dimensional. Under open-loop operating conditions, each tether, in the general case, will undergo flexural, extensional, and torsional deformations. Coupling between these modes of deformation and between modes of vibration of the rotor are to be expected. A similar device reported by Juneau *et al.* exhibited significant cross-axis sensitivity during open-loop resonant operation, which was attributed to elastic coupling [2]. The work of Juneau *et al.* and similar work by Ljung and Pisano [3] included inertial coupling, but assumed independent and uncoupled tethers, thereby ignoring elastic coupling.

One approach to avoiding the high levels reported for cross-axis sensitivity is to redesign the tethers so that the gyroscope has only one sense axis. However, such an approach would require two different proof masses in order to obtain two axes of sensitivity. Given that the cost of MEMS inertial instruments is approximately proportional to the surface area of the die on which it fits, there are strong economic reasons for research that can provide multiple sense axes from one proof mass. Thus, this work describes the detailed modeling of tether-based gyroscope suspensions in the hope of making these more compact designs more useful.

In this paper, after reviewing certain aspects of the rod theory developed by Green, Naghdi and their co-workers, a (nonlinear) mechanical model for the dual-axis gyroscope is developed. This model can be used to examine all features of the dynamics. We then specialize this model to a particular device, and examine three important modes. These modes are examined independently, however, in general they will be coupled.

In the interests of brevity, our discussion here is somewhat terse. Additional details and references can be found in our forthcoming work [4].

## Rod Theory of Green and Naghdi

The rod theory of Green and Naghdi is summarized in Naghdi [5]. It is a nonlinear theory, which is suited to numerous applications. We recall from his review that the rod is modeled by a material curve, and at each point of this curve a set of deformable vectors, known as directors, are attached. Here, we assume that the rod theory is one where there are two directors $\mathbf{d}_1$ and $\mathbf{d}_2$. The directors and the position vector $\mathbf{r}$ of points on the material curve are vector valued functions of $x_3$ and t, where $x_3$ is a convected coordinate and t is time. The values of these functions in a fixed reference configuration are $\mathbf{D}_1(x_3)$, $\mathbf{D}_2(x_3)$ and $\mathbf{R}(x_3)$ respectively.

The motion of the directed curve is governed by a set of balance laws. These laws are balance of mass, linear momentum, moment of momentum and director momenta. In the interests of brevity, we refer the reader to Naghdi [5] for a discussion of these matters. In addition, the balance laws are supplemented by constitutive relations. The relations for the linearized theory used in this paper are summarized in O'Reilly [6].

## A Model of a MEMS Gyroscope

We turn our attention now to a micromachined angular rate sensor, or gyroscope, shown in Figure 1. In what follows, we take subscripts on the left to identify tethers. The summation convention will be used on all other indices. Greek indices will be understood to range from 1 to 2, while Latin indices will range from 1 to 3, with the exception of Latin subscripts on the left which range from 1 to 4. Boldface type is used to indicate vectorial or tensorial quantities. The centroid of a surface defining the interface of the rotor and a tether is referred to as a "point of attachment."

The rotor is assumed to be a rigid body, so that the position of any material point associated with the rotor in a present configuration is given by

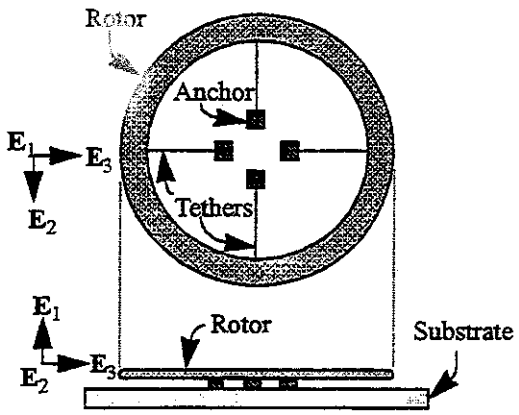


Figure 1: A micromachined dual-axis gyroscope design.

$$\mathbf{x}(\mathbf{X}, t) = \mathbf{Q}\mathbf{X} + \mathbf{q}, \tag{1}$$

where $\mathbf{X}$ is the vector to the material point when the rotor is in a fixed reference configuration, $\mathbf{Q}(t)$ is a rotation tensor, and $\mathbf{q}(t)$ is a vector. We define a set of fixed orthonormal basis vectors $\{\mathbf{E}_1,\mathbf{E}_2,\mathbf{E}_3\}$ which are coincident with the principal axes of inertia of the rotor.

It is convenient to define four sets of right-handed orthonormal bases, $\{{}_j\mathbf{A}_1,{}_j\mathbf{A}_2,{}_j\mathbf{A}_3\}$, such that:

$$\begin{aligned}
&{}_1\mathbf{A}_1 = \mathbf{E}_1, \quad {}_1\mathbf{A}_2 = \mathbf{E}_2, \quad {}_1\mathbf{A}_3 = \mathbf{E}_3,\\
&{}_2\mathbf{A}_1 = \mathbf{E}_1, \quad {}_2\mathbf{A}_2 = \mathbf{E}_3, \quad {}_2\mathbf{A}_3 = -\mathbf{E}_2,\\
&{}_3\mathbf{A}_1 = \mathbf{E}_1, \quad {}_3\mathbf{A}_2 = -\mathbf{E}_2, \quad {}_3\mathbf{A}_3 = -\mathbf{E}_3,\\
&{}_4\mathbf{A}_1 = \mathbf{E}_1, \quad {}_4\mathbf{A}_2 = -\mathbf{E}_3, \quad {}_4\mathbf{A}_3 = \mathbf{E}_2.
\end{aligned} \tag{2}$$

The corresponding co-rotational basis vectors are

$${}_j\mathbf{a}_i = \mathbf{Q}\,{}_j\mathbf{A}_i. \tag{3}$$

It is assumed that a straight reference configuration is available for each of the four tethers:

$${}_j\mathbf{D}_\alpha = {}_j\mathbf{D}_\alpha({}_jL, t) = {}_j\mathbf{A}_\alpha. \tag{4}$$

It is assumed that the length of the $j^{th}$ tether is ${}_jL$.

Next, we define the vector to the $j^{th}$ point of attachment in the reference configuration by ${}_j\mathbf{P}$:

$${}_j\mathbf{P} = \bar{\mathbf{X}} + {}_j\mathbf{S}, \tag{5}$$

where $\bar{\mathbf{X}}$ is the position vector of the rotor center of mass in the reference configuration, and ${}_j\mathbf{S}$ is the vector from the center of mass to the point of attachment. By (1), the vector to the $j^{th}$ point of attachment in the present configuration is given by

$${}_j\mathbf{p} = \bar{\mathbf{x}} + \mathbf{Q}\,{}_j\mathbf{S}, \tag{6}$$

where $\bar{\mathbf{x}}$ is the position vector of the center of mass.

The points of attachment are material points of both the tethers and the rotor:

$${}_j\mathbf{r}({}_jL, t) = {}_j\mathbf{p}, \; {}_j\mathbf{d}_\alpha({}_jL, t) = {}_j\mathbf{a}_\alpha. \tag{7}$$

The constraint forces and moments associated with these constraint equations can be obtained from a mechanical power balance (cf. [4]).

The balances of linear and angular momenta of the rotor are

$$\begin{aligned}
&-\sum_{j=1}^{4} {}_j\mathbf{n}({}_jL, t) = m_R\dot{\bar{\mathbf{v}}}\\
&-\sum_{j=1}^{4}\left({}_j\mathbf{p}\times{}_j\mathbf{n}({}_jL, t) + {}_j\mathbf{a}_\alpha\times{}_j\mathbf{m}^\alpha({}_jL, t)\right) = \dot{\overline{\mathbf{J}_R\boldsymbol{w}}},
\end{aligned} \tag{8}$$

where $m_R$ and $\mathbf{J}_R$ are the mass and inertia tensor of the rotor, respectively, and $\boldsymbol{w}$ is the rotor's angular velocity vector. The contact forces $\mathbf{n}$ and contact director forces $\mathbf{m}^\alpha$ in (8) are intrinsic to the rod theory that we are using.

The assigned forces and assigned director forces, which account for body forces and external forces, are assumed zero. The contact forces, intrinsic director forces $\mathbf{k}^\alpha$ and contact director forces are assumed to depend on the relative deformation [5]. To this end, we define the relative displacements ${}_j\mathbf{u}$ and ${}_j\delta_\alpha$ by:

$${}_j\mathbf{u} = {}_j\mathbf{r} - {}_j\mathbf{R}, \; {}_j\delta_\alpha = {}_j\mathbf{d}_\alpha - {}_j\mathbf{D}_\alpha, \tag{9}$$

with components

$${}_ju_i = ({}_j\mathbf{r} - {}_j\mathbf{R})\cdot{}_j\mathbf{A}_i, \; {}_j\delta_{\alpha i} = ({}_j\mathbf{d}_\alpha - {}_j\mathbf{D}_\alpha)\cdot{}_j\mathbf{A}_i. \tag{10}$$

Similarly, one has the representations of the form

$$\begin{aligned}
&{}_j\mathbf{n}({}_jL, t) = {}_jn_i({}_jL, t)\,{}_j\mathbf{A}_i,\\
&{}_j\mathbf{m}^\alpha({}_jL, t) = {}_jm_{\alpha i}({}_jL, t)\,{}_j\mathbf{A}_i.
\end{aligned} \tag{11}$$

The component forms of the balance laws for the directed curve used to model a tether can be written by taking their vector dot products with members of $\{{}_j\mathbf{A}_1,{}_j\mathbf{A}_2,{}_j\mathbf{A}_3\}$,

$$\begin{aligned}
&\frac{\partial}{\partial\,{}_jx_3}({}_jn_i) = {}_j\lambda({}_j\ddot{u}_i + {}_jy^{0\alpha}\,{}_j\ddot{\delta}_{\alpha i})\\
&\frac{\partial}{\partial\,{}_jx_3}({}_jm_{\alpha i}) - {}_jk_{\alpha i} = {}_j\lambda({}_jy^{0\alpha}\,{}_j\ddot{u}_i + {}_jy^{\alpha\beta}\,{}_j\ddot{\delta}_{\beta i}).
\end{aligned} \tag{12}$$

The component forms of and (9) will be written as needed.

For the gyroscope of interest, the tethers are assumed to have uniform rectangular cross-sections:

$$\begin{aligned}
&{}_jy^{01} = 0, \; {}_jy^{02} = 0, \; {}_jy^{21} = 0, \; {}_jy^{12} = 0,\\
&{}_jy^{11} = \frac{{}_jI_2}{{}_jA}, \; {}_jy^{22} = \frac{{}_jI_1}{{}_jA},
\end{aligned} \tag{13}$$

where ${}_jI_\alpha$ is the area moment of inertia of the $j^{th}$ tether

about the ${}_j\mathbf{A}_\alpha$ axis, and ${}_jA$ is the cross-sectional area of the $j^{th}$ tether. The mass per unit length ${}_j\lambda$ is

$$ {}_j\lambda = \rho\, {}_jA. \tag{14} $$

In the following we assume a sensor with the dimensions and material properties in Table 1. The constitutive relations we use for the contact forces, contact director forces and intrinsic director forces were established by Green and Naghdi and are summarized in [6]. The shear correction factor K we use is from Rubin [7].

Table 1: Design geometry and material properties.

| | |
|---|---|
| R = 250 um | Inner radius of rotor |
| L = 120 um | Tether length |
| h = 2.3 um | Tether/rotor thickness |
| w = 2.1 um | Tether width |
| E = 160 GPa | Young's modulus |
| v = 0.3 | Poisson's ratio |
| G = 61.5 GPa | Shear modulus |
| ρ = 2300 kg/m^3 | Density |
| K = 1 | Shear correction factor |

## Drive mode

We seek a solution of the governing equations with

$$ \boldsymbol{w} = \dot{\theta}_1 \mathbf{E}_1, \ \bar{\mathbf{x}} = 0, \tag{15} $$

which corresponds to free rotational vibrations of the rotor about the $\mathbf{E}_1$-axis.

Equations (7) can be written in terms of the relative displacements using (9) and (10), i.e.,

$$ \begin{aligned} &{}_ju_1({}_jL,t) = 0,\ {}_ju_2({}_jL,t) = -R\sin(\theta_1),\\ &{}_ju_3({}_jL,t) = R(\cos(\theta_1)-1),\ {}_j\delta_{1i}({}_jL,t) = 0,\\ &{}_j\delta_{21}({}_jL,t) = 0,\ {}_j\delta_{22}({}_jL,t) = \cos(\theta_1)-1,\\ &{}_j\delta_{23}({}_jL,t) = \sin(\theta_1). \end{aligned} \tag{16} $$

The component forms of the rotor momentum balances can be derived from with the assumed form of the motion. However, only one of the components of the balance of angular momentum is of interest:

$$ \begin{aligned} J_1\ddot{\theta}_1 = \sum_{j=1}^{4} &((R\,{}_jn_2({}_jL,t) - {}_jm_{23}({}_jL,t))\cos(\theta_1) + \\ &(R\,{}_jn_3({}_jL,t) + {}_jm_{22}({}_jL,t))\sin(\theta_1)). \end{aligned} \tag{17} $$

We can simplify (16) and (17) with a symmetry assumption:

$$ \begin{aligned} &{}_ju_2({}_jx_3,t) = u_2(x_3,t),\ {}_j\delta_{23}({}_jx_3,t) = \delta_{23}(x_3,t),\\ &{}_jL = L. \end{aligned} \tag{18} $$

Replacing trigonometric functions in (16) with the leading term in their series expansions, we obtain

$$ \begin{aligned} &u_1(L,t) = u_3(L,t) = 0, \quad u_2(L,t) = -R\theta_1,\\ &\delta_{1i}(L,t) = \delta_{2\alpha}(L,t) = 0,\ \delta_{23}(L,t) = \theta_1. \end{aligned} \tag{19} $$

Upon substitution of the constitutive relations for the linearized Green-Naghdi theory, (17)becomes

$$ \begin{aligned} J_1\ddot{\delta}_{23}(L,t) = 4\,[&-EI_1\delta'_{23}(L,t) + \\ &RGAK(\delta_{23}(L,t) + u'_2(L,t)) + \\ &\left(\frac{EA(1-\nu)}{(1+\nu)(1-2\nu)}u'_3(L,t) + \right. \\ &\left.\frac{EI_1}{2(1+\nu)}\delta'_{22}(L,t)\right)\delta_{23}(L,t)], \end{aligned} \tag{20} $$

where $(\,)'$ denotes the partial derivative with respect to $x_3$. We note that the variables $u_3$ and $\delta'_{22}$ in (20) are associated with axial and lateral extension. In order to remain consistent with the linearized Green-Naghdi theory, we neglect the nonlinear terms in (20), resulting in an equation dependent only on the relative displacements $u_2$ and $\delta_{23}$, which are associated with flexure. Therefore, we have the following set of equations governing the motion of the tethers and rotor:

$$ \begin{aligned} &GAK(\delta'_{23} + u''_2) = \lambda\ddot{u}_2\\ &EI_1\delta''_{23} - GAK(\delta_{23} + u'_2) = \lambda y^{22}\ddot{\delta}_{23}\\ &u_2(0,t) = 0, \delta_{23}(0,t) = 0,\ u_2(L,t) = -R\delta_{23}(L,t),\\ &J_1\ddot{\delta}_{23}(L,t) = 4\cdot[RGAK(\delta_{23}(L,t) + \\ &\qquad u'_2(L,t)) - EI_1\delta'_{23}(L,t)], \end{aligned} \tag{21} $$

and we conclude that to a linear approximation, flexural deformations are decoupled from other deformations.

Equations (21) are similar to the equations governing planar deformations of Timoshenko beams. We remark that several authors have recently considered the vibrations of such beams with an added tip mass (e.g., [8], [9], [10]). Turcotte [11] has investigated the free flexural and extensional vibrations of unloaded cantilever beams in the context of the Green-Naghdi theory. The problem of the gyroscope differs from these examples because of the constrained motion of the rigid body, but many developments that follow are parallel.

We assume a separation of variables:

$$ \begin{aligned} &u_2(x_3,t) = U_2(x_3)\sin(\omega_D t)\\ &\delta_{23}(x_3,t) = \Delta_{23}(x_3)\sin(\omega_D t). \end{aligned} \tag{22} $$

Substituting these expressions into (21) yields ordinary differential equations for $U_2(x_3)$ and $\Delta_{23}(x_3)$, which are satis-

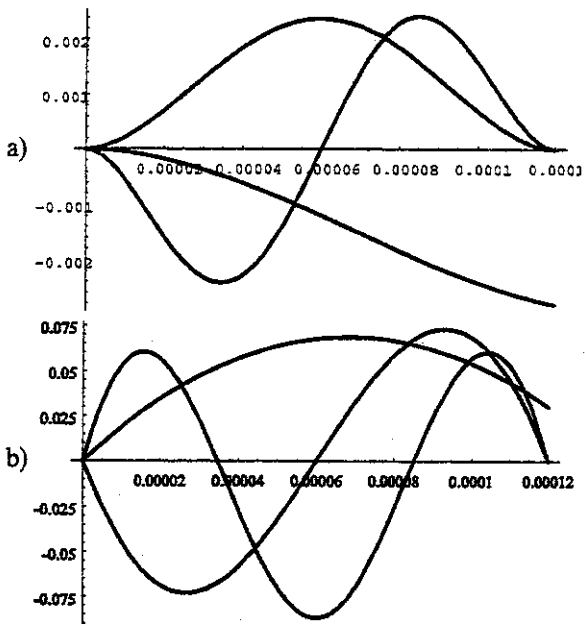


Figure 2: Drive mode: a) first three mode shapes $U_2(x_3)$, and b) first three mode shapes $\Delta_{23}(x_3)$.

fied by

$$\begin{aligned} U_2(x_3) &= A_1\cos(p_1x_3) + A_2\sin(p_1x_3) + \\ &A_3\cosh(p_2x_3) + A_4\sinh(p_2x_3), \\ \Delta_{23}(x_3) &= B_1\cos(p_1x_3) + B_2\sin(p_1x_3) + \\ &B_3\cosh(p_2x_3) + B_4\sinh(p_2x_3). \end{aligned} \tag{23}$$

Of the eight coefficients in 23, only four are independent. The relations between the coefficients can be found in [8], [9], [10], or [11].

The eigenvalues $p_1$ and $p_2$ are given by

$$p_{1,2}^2 = \frac{\lambda\omega_D^2}{2GAKEI_1}\left[EI_1 + GAKy^{22} \pm \left(\left(EI_1 + GAKy^{22}\right)^2 - 4GAKEI_1\left(y^{22} - \frac{GAK}{\lambda\omega_D^2}\right)\right)^{\frac{1}{2}}\right]. \tag{24}$$

Using three boundary conditions, three of the unknown coefficients can be eliminated. The remaining boundary condition yields the frequency equation, the roots of which are the natural frequencies. Once the natural frequencies are calculated, the associated mode shapes are found by setting one of the coefficients equal to one, say, and computing the remaining coefficients. The scale of the mode shapes plotted in this paper is therefore arbitrary, although in general it is possible to normalize mode shapes using an orthonormality condition.

The first three drive mode shapes for the gyroscope are shown in Figure 2. The fundamental natural frequency of 14.7 kHz agrees well with the experimentally measured value of 13.7 kHz [12].

## Tilt mode

We seek a solution of the governing equations with

$$\boldsymbol{w} = \dot{\theta}_2\mathbf{E}_2,\ \bar{\mathbf{x}} = \mathbf{0}, \tag{25}$$

corresponding to free rotational vibrations of the rotor about the $\mathbf{E}_2$-axis.

We employ a similar procedure as that used for the drive mode case. The assumed symmetries are

$$\begin{aligned} {}_1u_1({}_1x_3, t) &= -{}_3u_1({}_3x_3, t) = u_1(x_3, t), \\ {}_1\delta_{13}({}_1x_3, t) &= -{}_3\delta_{13}({}_3x_3, t) = \delta_{13}(x_3, t), \\ {}_2\delta_{12}({}_2x_3, t) &= -{}_4\delta_{12}({}_4x_3, t) = \delta_{12}(x_3, t), \\ {}_2\delta_{21}({}_2x_3, t) &= -{}_4\delta_{21}({}_4x_3, t) = \delta_{21}(x_3, t). \end{aligned} \tag{26}$$

Upon linearizing, we obtain the following set of governing equations:

$$\begin{aligned} &GAK(\delta'_{13} + u''_1) = \lambda\ddot{u}_2, \\ &EI_1\delta''_{13} - GAK(\delta_{13} + u'_1) = \lambda y^{22}\ddot{\delta}_{13}, \\ &\frac{D}{2}\delta''_{12} = \lambda y^{11}\ddot{\delta}_{12},\ \frac{D}{2}\delta''_{21} = \lambda y^{22}\ddot{\delta}_{21}, \\ &u_1(0, t) = 0,\ \delta_{12}(0, t) = 0,\ \delta_{13}(0, t) = 0, \\ &\delta_{21}(0, t) = 0,\ u_1(L, t) = -R\,\delta_{13}(L, t), \\ &\delta_{12}(L, t) = -\delta_{21}(L, t),\ \delta_{12}(L, t) = \delta_{13}(L, t), \\ &J_2\ddot{\delta}_{13}(L, t) = 2\cdot[RGAK(\delta_{13}(L, t) + \\ &\qquad u'_1(L, t)) - EI_2\,\delta'_{13}(L, t) + \\ &\qquad D(\delta'_{12}(L, t) + \delta'_{21}(L, t))], \end{aligned} \tag{27}$$

where $D$ is the torsional rigidity, given by [13] as

$$D = Ghw^3\left(\frac{1}{3} - 0.21\frac{w}{h}\left(1 - \frac{w^4}{12h^4}\right)\right). \tag{28}$$

Equations (27) are consistent with two tethers undergoing flexural deformations and the others undergoing torsional deformations.

We assume a separation of variables:

$$\begin{aligned} u_1(x_3, t) &= U_1(x_3)\sin(\omega_T t), \\ \delta_{13}(x_3, t) &= \Delta_{13}(x_3)\sin(\omega_T t), \\ \delta_{12}(x_3, t) &= \Delta_{12}(x_3)\sin(\omega_T t), \\ \delta_{21}(x_3, t) &= \Delta_{21}(x_3)\sin(\omega_T t). \end{aligned} \tag{29}$$

Substituting, we obtain

$$
\begin{aligned}
U_1(x_3) &= A_1\cos(p_1x_3) + A_2\sin(p_1x_3) + \\
&\quad A_3\cosh(p_2x_3) + A_4\sinh(p_2x_3), \\
\Delta_{13}(x_3) &= B_1\cos(p_1x_3) + B_2\sin(p_1x_3) + \\
&\quad B_3\cosh(p_2x_3) + B_4\sinh(p_2x_3), \\
\Delta_{12}(x_3) &= C_1\cos(q_1x_3) + C_2\sin(q_1x_3), \\
\Delta_{21}(x_3) &= D_1\cos(q_2x_3) + D_2\sin(q_2x_3),
\end{aligned} \tag{30}
$$

where again the coefficients $A_i$ and $B_i$ ($i = 1,...,4$) are related. The eigenvalues are

$$
p_{1,2}^2 = \frac{\lambda\omega_T^2}{2GAKEI_2}\left[EI_2 + GAKy^{11} \pm \left(\left(EI_2 + GAKy^{11}\right)^2 - 4GAKEI_2\left(y^{11} - \frac{GAK}{\lambda\omega_T^2}\right)\right)^{\frac{1}{2}}\right],
$$

$$
q_1 = \sqrt{\frac{2\lambda\omega_T^2\, y^{11}}{D}},\ q_2 = \sqrt{\frac{2\lambda\omega_T^2\, y^{22}}{D}}. \tag{31}
$$

Thus, there are eight independent coefficients associated with the solution, seven of which can be eliminated using seven of the boundary conditions of (28). The roots of the remaining boundary condition equation are the natural frequencies. As for the case of the drive mode, the mode shapes can be found by setting one of the coefficients to unity and solving for the rest.

The first three tilt mode shapes for the gyroscope are shown in Figure 3. The fundamental natural frequency of 16.3 kHz is slightly higher than the experimentally measured value of 15 kHz [12], possibly because of the electrostatic forces between the rotor and capacitive sense pads on the substrate, which act like negative spring forces. The linear shape of the first three torsional modes indicates that torsional stiffness is a secondary contributor to the overall stiffness, which is dominated by flexural effects.

## Bounce mode

We seek a solution of the governing equations with

$$
\mathbf{Q} = \mathbf{I},\ \bar{\mathbf{x}} = X\sin(\omega_B t)\,\mathbf{E}_1, \tag{32}
$$

where $\mathbf{I}$ is the identity tensor. This motion corresponds to free translational oscillations of the rotor parallel to the $\mathbf{E}_1$-axis with frequency $\omega_B$ and amplitude X.

The assumed symmetries are

$$
{}_ju_1({}_jx_3, t) = u_1(x_3, t),\ {}_j\delta_{13}({}_jx_3, t) = \delta_{13}(x_3, t). \tag{33}
$$

The component forms of the linearized governing equations are

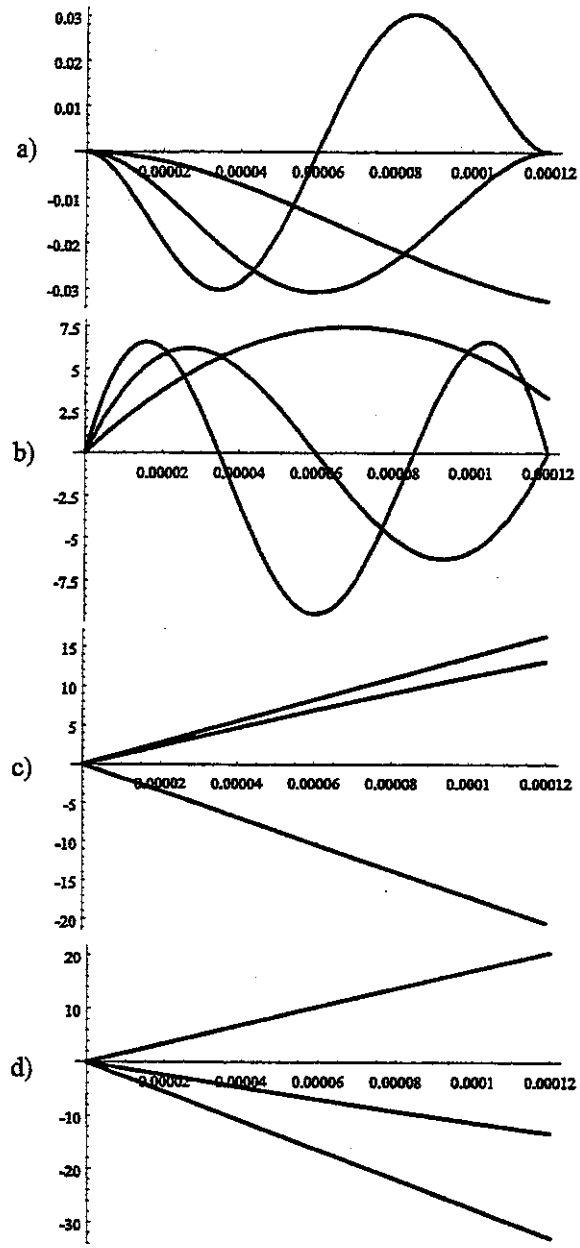


Figure 3: Tilt mode: a) first three mode shapes $U_1(x_3)$, b) first three mode shapes $\Delta_{13}(x_3)$, c) first three mode shapes $\Delta_{12}(x_3)$, and d) first three mode shapes $\Delta_{21}(x_3)$.

$$
\begin{aligned}
&GAK(\delta'_{13} + u''_1) = \lambda\,\ddot{u}_1, \\
&EI_1\delta''_{13} - GAK(\delta_{13} + u'_1) = \lambda y^{22}\ddot{\delta}_{23}, \\
&u_1(0,t) = 0,\ \delta_{13}(0,t) = 0,\ \delta_{13}(L,t) = 0, \\
&4\cdot GAK(\delta_{13}(L,t) + u'_1(L,t)) = m_R\,\ddot{u}_1(L,t).
\end{aligned} \tag{34}
$$

Again, we assume a separation of variables:

$$u_1(x_3,t) = U_1(x_3)\sin(\omega_B t),$$
$$\delta_{13}(x_3,t) = \Delta_{13}(x_3)\sin(\omega_B t). \quad (35)$$

The eigenvalues for this case are given by $(31)_1$.

The first three bounce mode shapes are shown in Figure 4. The fundamental natural frequency of 25.2 kHz is substantially higher than the experimentally measured frequency of 17.4 kHz [12], probably due to electrostatic attraction between the rotor and sense pads.

## Conclusions

The application of a non-linear, three-dimensional theory of rods to the vibrations of a dual-axis MEMS gyroscope has been investigated. The advantage of the theory is that it identifies the form of the coupling between flexural, torsional, and extensional modes of deformation. Upon linearization of the governing equations, one obtains equations similar to those arising in Timoshenko beam theory for the free vibrations of the gyroscope in its drive and bounce modes. However, these linearized equations differ from those derived from beam theory in that the tilt mode vibration equations describe two tethers in flexural vibrations with the remaining two tethers in torsional vibrations, with both types of deformations accounted for in the same theory. The calculated values of the natural frequencies of the first modes are not significantly different from those obtained using Euler-Bernoulli beam theory. However, we note that for the designed operation of a dual-axis gyroscope, the drive and tilt modes are present simultaneously, and will therefore interact. In addition, geometrical imperfections will produce coupling between modes. This work provides a stepping stone toward analyzing these more complicated effects.

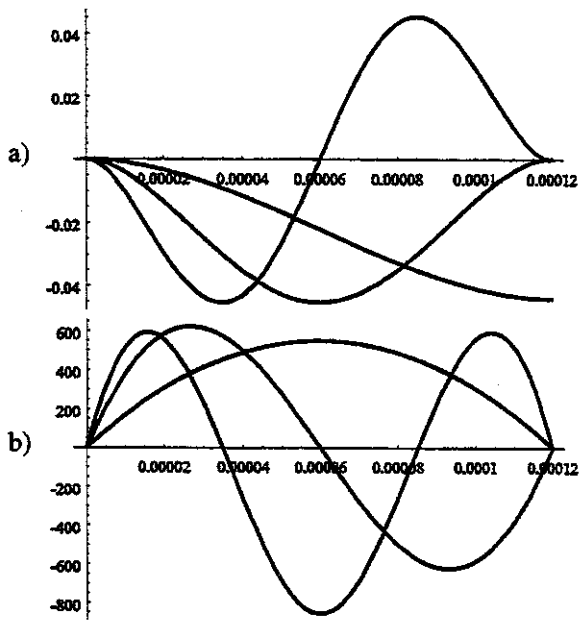


Figure 4: Bounce mode: a) first three mode shapes $U_1(x_3)$, and b) first three mode shapes $\Delta_{13}(x_3)$.

## Acknowledgments

The authors wish to thank Professor Oliver M. O'Reilly of the Department of Mechanical Engineering at U. C. Berkeley for his generous assistance with this paper. This work was supported under DARPA grant F30602-97-2-0266.

## References

1. Juneau, T., Doctoral Thesis, Dept. of Mechanical Engineering, U. C. Berkeley, 1998.
2. Juneau, T., Pisano, A. P., and Smith, J. H., "Dual-axis operation of a micromachined rate gyroscope," Transducers '97, Chicago, IL, June 16-19, 1997.
3. Ljung, P. B. and Pisano, A. P., "Nonlinear dynamics of micromachined rate gyros," DSC-vol. 59, Microelectromechanical Systems (MEMS), ASME 1996.
4. Davis, W. O. and Pisano, A. P., "Analysis of free vibrations and elastic coupling of a MEMS gyroscope," in preparation.
5. Naghdi, P. M., "Finite deformation of elastic rods and shells," Proceedings of the IUTAM Symposium on Finite Elasticity, Bethlehem, PA, 1980, eds. D. E. Carlson and R. T. Shield, pp. 47-103. Martinus Nijhoff, The Hague.
6. O'Reilly, O. M., "On constitutive relations for elastic rods," International Journal of Solids and Structures, v. 35, 1998, pp. 1009-1024.
7. Rubin, M. B., "Restrictions on nonlinear constitutive relations for elastic rods," Journal of Elasticity, v. 44, pp. 9-36, 1996.
8. Bruch, J. C. and Mitchell, T. P., "Vibrations of a mass-loaded clamped-free Timoshenko beam," Journal of Sound and Vibration, v. 114, 1987, pp. 341-345.
9. Abramovich, H. and Hamburger, O., "Vibration of a cantilever Timoshenko beam with a tip mass," Journal of Sound and Vibration, v. 148, 1991, pp. 162-170.
10. White, M. W. D. and Heppler, G. R., "Vibration modes and frequencies of Timoshenko beams with attached rigid bodies," ASME Journal of Applied Mechanics, v. 62, pp. 193-199, March, 1995.
11. Turcotte, J. S., Approximate theories of elastic rods with applications, Doctoral Thesis, Dept. of Mechanical Engineering, U. C. Berkeley, 1997.
12. Juneau, T., personal communication.
13. Roark, R. J. and Young, W. C., Formulas for stress and strain, McGraw-Hill, 1975.